ACS APPLIED MATERIALS & INTERFACES

Research Article

www.acsami.org

An Ambipolar BODIPY Derivative for a White Exciplex OLED and Cholesteric Liquid Crystal Laser toward Multifunctional Devices

Marian Chapran,[†,‡] Enrico Angioni,[§] Neil J. Findlay,[§] Benjamin Breig,[§] Vladyslav Cherpak,[⊥] Pavlo Stakhira,[‡] Tell Tuttle,[§] Dmytro Volyniuk,[∥] Juozas V. Grazulevicius,[∥] Yuriy A. Nastishin,[⊥] Oleg D. Lavrentovich,[*,⊥] and Peter J. Skabara[*,§]

[†]Department of Molecular Physics, Lodz University of Technology, Zeromskiego 116, 90-924 Lodz, Poland

[‡]Lviv Polytechnic National University, S. Bandera 12, 79013 Lviv, Ukraine

[§]WestCHEM, Department of Pure and Applied Chemistry, University of Strathclyde, Glasgow G1 1XL, U.K.

[∥]Department of Polymer Chemistry and Technology, Kaunas University of Technology, Radvilenu Plentas 19, LT-50254 Kaunas, Lithuania

[⊥]Liquid Crystal Institute and Chemical Physics Interdisciplinary Program, Kent State University, Kent, Ohio 44242, United States

Supporting Information

ABSTRACT: A new interface engineering method is demonstrated for the preparation of an efficient white organic light-emitting diode (WOLED) by embedding an ultrathin layer of the novel ambipolar red emissive compound 4,4-difluoro-2,6-di(4-hexylthiopen-2-yl)-1,3,5,7,8-pentamethyl-4-bora-3*a*,4*a*-diaza-*s*-indacene (bThBODIPY) in the exciplex formation region. The compound shows a hole and electron mobility of 3.3×10^{-4} and 2×10^{-4} cm^2 V^{-1} s^{-1}, respectively, at electric fields higher than 5.3×10^5 V cm^{-1}. The resulting WOLED exhibited a maximum luminance of 6579 cd m^{-2} with CIE 1931 color coordinates (0.39; 0.35). The bThBODIPY dye is also demonstrated to be an effective laser dye for a cholesteric liquid crystal (ChLC) laser. New construction of the ChLC laser, by which a flat capillary with an optically isotropic dye solution is sandwiched between two dye-free ChLC cells, provides photonic lasing at a wavelength well matched with that of a dye-doped planar ChLC cell.

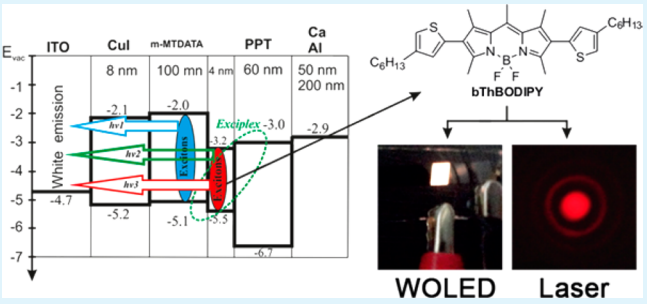

KEYWORDS: *organic light-emitting diodes (OLEDs), white light, exciplex, BODIPY dye, cholesteric liquid crystal (ChLC) laser*

INTRODUCTION

Recently, white organic light-emitting diodes (WOLEDs) have attracted the attention of the scientific community for their promising application in lighting technologies.[1−3] The fundamental parameters that determine the performance of WOLEDs in display technologies and lighting systems are the power efficiency, color chromaticity, and the cost of manufacturing. Already there are competitive technologies that have enabled successful improvement of these parameters, such as phosphorescent WOLEDs, which have dominated in terms of efficiency.[2,4,5] Usually, this type of WOLED is based on the use of guest (phosphorescent metal−organic complexes) and host materials[4] but can be associated with some technical challenges including issues determining an appropriate concentration of the guest in the host system and the engineering of appropriate multilayer sandwich device configurations.[4,5] Moreover, the host and phosphorescent materials should be designed with suitable triplet and singlet energy levels, especially considering the energies of the blue luminescent component.[5] In 2013, Zhao et al.[6] proposed an alternative device architecture that utilized an ultrathin (0.1 nm) phosphorescent nondoped emissive layer for the formation of a highly efficient phosphorescent WOLED. However, such an approach does not provide a satisfactory efficiency roll-off which is especially important for the development of attractive lighting systems.[7]

One of the most simple and conceptual approaches for the development of WOLEDs is the introduction of yellow emission generated by an exciplex (bimolecular excited species). This emission can be used in combination with blue emission from a fluorescent excited state[8−10] or from a second exciplex state, as described recently by Chou and co-workers.[11] Exciplex-type OLEDs are characterized by high values of external quantum efficiency due to the intramolecular spin up-conversion from the nonradiative triplet excited state to the singlet excited state (thermally activated delayed fluorescence (TADF)).[11,12] Despite the high efficiency of all-exciplex-based OLEDs, the main limiting factor in the development of a real

Received: October 26, 2016
Accepted: January 12, 2017
Published: January 12, 2017

DOI: 10.1021/acsami.6b13689
ACS Appl. Mater. Interfaces 2017, 9, 4750−4757

white OLED is the limited number of known materials that can form exciplexes with emission in the blue and red regions of the visible spectrum.[11−13] Recently, exciplexes have been used as hosts for highly efficient yellow and red fluorescent OLEDs[14] as well as for blue phosphorescent OLEDs.[15] The energy transfer from the exciplexes to the dopants was efficient with no significant energy loss.[15] Long-range exciplex emission was observed recently in spatially separated electron-donating and electron-accepting molecules across an ultrathin spacer layer.[16]

Here we present a novel red emitter, 4,4-difluoro-2,6-di(4-hexylthiopen-2-yl)-1,3,5,7,8-pentamethyl-4-bora-3*a*,4*a*-diaza-*s*-indacene (bThBODIPY), that was synthesized using an adapted literature procedure.[17,18] 4,4-Difluoro-4-bora-3*a*,4*a*-diaza-*s*-indacene (BODIPY) derivatives are characterized by small Stokes shifts, high thermal and photochemical stabilities, high photoluminescence quantum yields (PLQYs), good solubility, and general chemical robustness.[19,20] They have been used as organic semiconductors for different applications, including OLEDs, OPVs, OFETs, and lasers,[21] as well as finding applications as biochemical labels, fluorescent switches, and chemosensors.[20] In bThBODIPY, the thiophene substituents are electron-rich and the BODIPY unit is electron-deficient, resulting in a donor−acceptor structure. Alkyl chains were introduced with the aim to increase the solubility of the new material in common organic solvents (and hence their processability) and to avoid intermolecular packing. In fact, BODIPY molecules, due to their planarity,[22] commonly exhibit "aggregation-caused quenching (ACQ)" effects: showing strong fluorescence in dilute solution but weaker luminescence in the solid state.[23−26] In such a molecule, the efficiency of the energy transfer through the BODIPY core is generally increased,[27] producing an elevated PLQY as demonstrated in similar *β*-substituted BODIPY molecules.[28,29] Here, we present a new interface engineering method for the preparation of efficient white OLEDs by embedding an ultrathin layer of the new highly efficient fluorescent red emitter bThBODIPY in the exciplex formation region. The resulting WOLED presented a combined emission from different excited states: red exciton emission from the ultrathin bThBODIPY film, green emission from the *m*-MTDATA (4,4′,4″-tris[phenyl(*m*-tolyl)amino]-triphenylamine)/ PPT (2,8-bis(diphenylphosphoryl)dibenzo-[*b*,*d*]thiophene) exciplex, and blue emission from *m*-MTDATA excitons and excimer. A prerequisite for the implementation of this approach is a theoretical model for the electronic processes at the organic exciplex interfaces, which shows that the intermolecular excited state may form even if the donor and acceptor layers are separated.[30,31] The compounds *m*-MTDATA and PPT have been employed here in order to obtain a green exciplex based emission. This strategy has been previously applied in the fabrication of different OLEDs and demonstrated one of the highest external quantum yields (10%) reported.[10] The outstanding fluorescence characteristics of the dye bThBODIPY can also be exploited for laser generation in cholesteric liquid crystals (ChLC). Two experimental approaches for optically pumped mirrorless lasing in a dye-doped ChLC have been tested. In the first approach, laser generation was examined in a conventional geometry, where the dye-doped ChLC was filled into a flat cell with tangential alignment of the ChLC molecules at (helical axis normal to) the cell substrates (from herein referred to as the planar cell). In the second approach, a flat microcapillary filled with a toluene solution of bThBODIPY was placed between two flat planar dye-free ChLC cells. Toluene was chosen as a solvent since it evaporates relatively slowly in comparison with other solvents, and this is known to provide good quality, uniform films. Stable optically pumped lasing was achieved with both approaches.

RESULTS AND DISCUSSION

Synthesis. The emissive bThBODIPY material was obtained in 34% yield by Stille coupling between 4,4-difluoro-2,6-diiodo-1,3,5,7,8-pentamethyl-4-bora-3*a*,4*a*-diaza-*s*-indacene and (4-hexylthiophen-2-yl)trimethylstannane using tetrakis-(triphenylphosphine)palladium(0) as the catalyst (Figure 1; see Figures S1 and S2 for NMR data). The compound bThBODIPY was obtained as a dark red solid that easily formed films from concentrated solutions in common organic solvents (e.g., dichloromethane, chloroform, ethyl acetate). The material is thermally stable up to ca. 320 °C, as shown by TGA analysis (Figure S3).

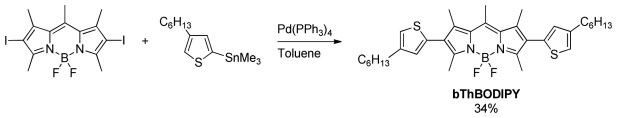

Figure 1. Synthesis of bThBODIPY.

Electronic Properties and Theoretical Calculations. The absorption and emission spectra of the solution (10^{-5} M in CH_2Cl_2) and of the vacuum-deposited film of bThBODIPY were recorded (Figure 2). The absorption spectrum of the solution showed four bands with maxima at 524, 394, 277, and

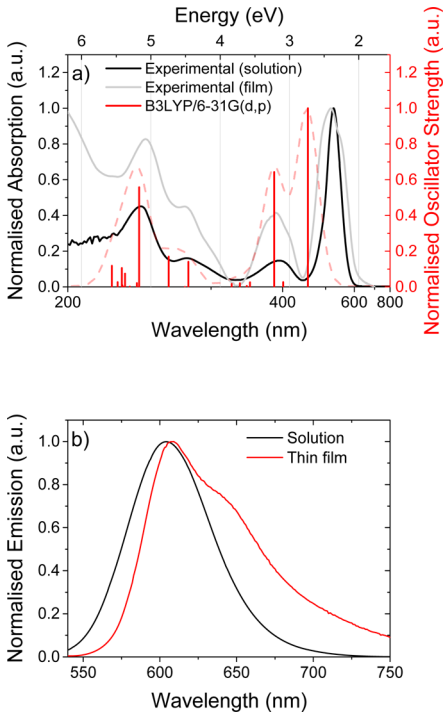

Figure 2. (a) Experimental UV−vis absorption spectra in solution (10^{-5} M in CH_2Cl_2, black) and for the vacuum deposited film (gray) of bThBODIPY, calculated vertical absorptions (red) and Gaussian fitted (fwhm = 0.37 eV) absorption spectra at the TD-DFT/PBE0/6-311G(d,p) level of theory (dashed red) on the vacuum-deposited film of bThBODIPY. (b) Photoluminescence spectra in solution (10^{-5} M in CH_2Cl_2, black) and for the vacuum deposited film of bThBODIPY.

DOI: 10.1021/acsami.6b13689
ACS Appl. Mater. Interfaces 2017, 9, 4750−4757

241 nm, while the solid sample exhibited maxima at 516, 387, 275, and 244 nm. The slight blue-shift of the film spectrum is due to the general larger population of the less energetic vibrational states due to the smaller reorganization energy in the solid state.[32] However, the edge of the lowest energy absorption band of the film showed a red-shift when compared with that of the solution. The sharp profile of the less energetic band is characteristic of the BODIPY unit of the molecule,[27] whereas the other bands have charge transfer character between the donor and the acceptor components, as observed for similar BODIPY derivatives.[29,33] From the longest wavelength absorption edge of the UV−vis absorption spectra in solution, it was possible to calculate an optical HOMO−LUMO gap of 2.2 eV. The fluorescence spectra showed a main band, with a large Stokes shift, centered at 605 and 609 nm for the solution and the film of bThBODIPY, respectively. In the spectrum of the film, the main emission was associated with a shoulder centered at ca. 636 nm, which is likely due to intermolecular interactions between the bThBODIPY molecules that are more likely to occur in the solid state.[34] Fluorescence decay measurements (recorded at 605 nm) were performed for a vacuum-deposited film of bThBODIPY. A single-exponential decay profile was observed, resulting in a lifetime of 2.21 ns that can be assigned to pure fluorescence emission.[35,36] The decay spectrum recorded at 650 nm shows a fluorescence emission with a decay time of 0.92 ns, in agreement with the emission arising from the $\pi-\pi$ stacking in the film (Figure S4). Absolute photoluminescence quantum yields (PLQYs) of 97% and 17% were obtained for the dichloromethane solution and for the thin film (vacuum deposition at 10^{-6} Torr) of bThBODIPY, respectively.

To explain the experimentally observed electronic spectra (and the electrochemical behavior), quantum chemical calculations were performed for bThBODIPY using density functional theory (DFT) and its time-resolved counterpart (TD-DFT).[37,38] All the calculations were performed with the software package Gaussian09 (Revision A.02),[39] with the hexyl chains replaced with methyl groups to limit the computational cost without compromising the integrity of the calculations. The geometry of bThBODIPY was optimized at the B3LYP/6-311G(d,p) level of theory, and the analysis of the vibrational frequencies revealed the location of the sought-for energy minimum. The BODIPY unit is planar as expected, but the thiophene substituents are rotated by ca. 60° out of the plane of the core. The wave function of the HOMO orbital is delocalized over the whole π-backbone of the molecule, but the LUMO wave function is mainly localized on the BODIPY unit (Figure S5 and Table S1). The first 20 singlet vertical transitions were calculated for bThBODIPY in the vacuum using the TD-DFT/B3LYP/6-311G(d,p) level of theory (Figure S5 and Table S2). The first two calculated vertical transitions with significant oscillation strength were at 2.73 and 3.22 eV, corresponding to the experimental absorption bands at ca. 2.40 and 3.20 eV (516 and 387 nm) in the solid state (524 and 394 nm in solution). These are transitions between the HOMO and HOMO−2 orbitals (ground states), delocalized over the whole molecule and the LUMO (excited state), mainly localized on the central BODIPY unit (Figure 3 and Figure S5). The other significant transitions that correspond to the band centered at 4.51 and 5.08 eV in the solid state (277 and 241 nm in solution) are mainly represented by vertical transitions at 4.46 and 5.17 eV. They are between orbitals delocalized over the entire molecule (HOMO, HOMO−1, HOMO−2) and

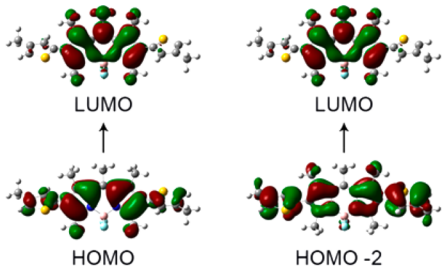

Figure 3. Graphical representation of the HOMO to LUMO and HOMO−2 to LUMO vertical transitions (isosurfaces 0.020) calculated at the B3LYP/6-311G(d,p) level of theory for bThBODIPY.

orbitals mainly localized on the thiophene substituents (LUMO +1, LUMO+2). This is in agreement with the donor−acceptor character desired for bThBODIPY and confirmed experimentally by the electrochemical data; i.e., the thiophene substituents act as donors and the BODIPY center as an acceptor. The calculated energies are generally in good agreement with the experimental data, in particular with the absorption data obtained with the thin film where there are no additional solvent effects.

The cyclic voltammograms of bThBODIPY (Figure 4) showed a reversible reduction process ($E_{1/2}$ = −1.63 V)

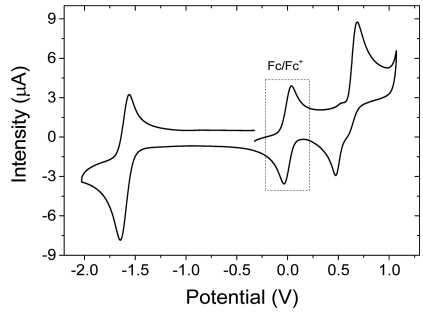

Figure 4. Cyclic voltammograms of bThBODIPY (10^{-4} M in CH_2Cl_2 with ferrocene as the internal standard). The measurements were performed using a glassy carbon working electrode, Ag/AgCl reference electrode, and platinum wire counter electrode. The supporting electrolyte was 0.1 M tetrabutylammonium hexafluorophosphate in dichloromethane. All the waves were referenced to ferrocene.

attributable to the typical formation of a radical anion on the BODIPY unit.[40−42] The oxidation waves showed a quasi-reversible process at $E_{1/2}$ = +0.60 V. These are due to the electron donor character of the 4-hexylthiophen-2-yl units.[40−42] The electrochemical HOMO and LUMO levels were calculated from the onset of the first oxidation wave (−5.5 eV) and reduction wave (−3.2 eV), respectively (the data were referenced to ferrocene, which has a HOMO of −4.8 eV). The electrochemical HOMO−LUMO gap was therefore determined to be 2.3 eV.

Solid-State Photoelectrical Properties of bThBODIPY. Since solid-state layers of bThBODIPY are required for the fabrication of OLEDs, an ionization potential (IP) of 5.68 eV was measured by electron photoemission experiments on the vacuum-deposited film of bThBODIPY (Figure S6). The IP is in good agreement with the result obtained by DFT calculations ($HOMO^{DFT}$ = −5.6 eV) and from the electrochemical experiments ($HOMO^{EL}$ = −5.5 eV). The slight disagreement with the $HOMO^{EL}$ is likely due to intermolecular interactions (stacking) of bThBODIPY that can occur in the

DOI: 10.1021/acsami.6b13689
ACS Appl. Mater. Interfaces 2017, 9, 4750−4757

solid film. The charge-transport properties of the bThBODIPY film were studied by the time-of-flight (TOF) technique. The TOF charge mobilities (μ) were calculated using the formula $\mu = d^2/(V \times t_{tr})$,[43] where d is the thickness of the layer, V is the applied voltage to the samples, and t_{tr} is the transit time, which was taken from the photocurrent transients plotted in log−log scales (Figure 5, insets). Transit times for both holes and

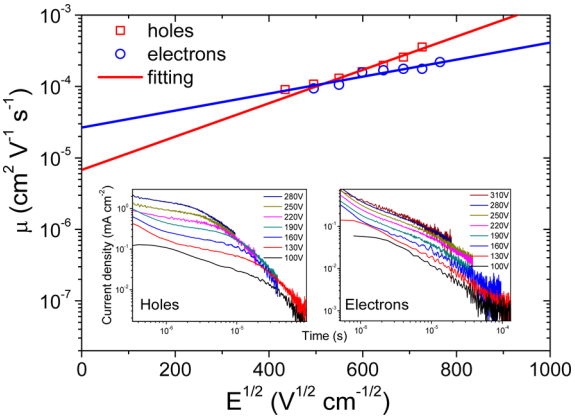

Figure 5. Electric field dependences of hole and electron mobilities for the layer of bThBODIPY. Insets: the hole and electron TOF transient curves for bThBODIPY in log−log scales.

electrons were determined demonstrating the ambipolar nature of the material and allowing the estimation of the hole and electron mobilities of bThBODIPY. The electric field dependencies of hole and electron mobilities showed linear dependencies on the square root of the electric field ($E^{1/2}$). This observation is in agreement with the Poole−Frenkel relationship $\mu = \mu_0 \times \exp(\alpha \times E^{1/2})$ (Figure 5).[44] Hole and electron mobilities of the vacuum-deposited layer of bThBODIPY were found to be 3.3×10^{-4} and 2.0×10^{-4} cm^2 V^{-1} s^{-1}, respectively, at electric fields higher than 5.3×10^5 V cm^{-1} (Figure 5). Such moderate values of charge mobilities are comparable to many light-emitting materials used in OLEDs.[45] The hole and electron mobilities of bThBODIPY are well balanced, showing that this new compound can be used as an emitting layer in OLEDs.

Device Fabrication. Two devices were fabricated by successive vacuum deposition of organic semiconductor layers and metal electrodes onto precleaned indium tin oxide (ITO)-coated glass substrates under a vacuum of 10^{-5} Torr. The structures of the devices were (A) ITO/CuI(8 nm)/*m*-MTDATA(20 nm)/bThBODIPY(70 nm)/PPT(25 nm)/Ca(50 nm)/Al(200 nm) and (B) ITO/CuI(8 nm)/*m*-MTDATA(100 nm)/bThBODIPY(4 nm)/PPT(60 nm)/Ca(50 nm)/Al(200 nm) (Figure S7). The active area of the WOLEDs was 3×2 mm^2, and the characteristics of the devices were obtained immediately after fabrication without further passivation in air. CuI was used as the hole-transporting layer.[46] The laser generation was tested in an assembled cell with a gap thickness of 50 μm, filled with a dye-doped cholesteric mixture. The cholesteric mixture used was prepared including 27.6 wt % of the chiral dopant S811 (Merck) in a nematic liquid crystal of ZLI-2248 (Merck) doped with 0.3 wt % of the bThBODIPY dye. Planar alignment of the cholesteric molecules at the cell substrate was obtained with the PI-2555 polymer layer spin-coated onto glass substrates. A second-harmonic light beam from a pulse Q-switched Nd:YAG laser (from CryLas532Q) focused with a lens was used for the excitation of the cell at the beam incidence angle of 45°. The wavelength of the pumping light was 532 nm with a pulse width of 1 ns and pulse energy up to 2 μJ pulse^{-1}. Lasing was stable at different pulse repetition rates ranging from 2 Hz to 1 kHz with the maximum output at the repetition rate of approximately 100 Hz. The lasing emission was collected in the direction perpendicular to the substrates. The emission spectra were measured using a fiber-based spectrometer (Ocean Optics USB2000). A Molectron OPTIMUM 4001 laser energy meter was used for measuring the lasing threshold. For the capillary laser construction, a 0.3 wt % solution of bThBODIPY dye in toluene was placed into a rectangular 2×0.1 mm^2 VitroCom glass capillary, the ends of which were sealed with epoxy resin. The capillary was placed between two identical cholesteric (27.6 wt % of S811 in ZLI-2248) cells of 20 μm gap formed by glass substrates covered with a PI-2555 layer for a planar alignment. The capillary was covered with a thin layer of optical glue Norland 64 for refractive index matching and tightly assembled between the ChLC cells. The whole construction could be easily assembled/disassembled with replaceable ChLC cells and capillaries.

OLED Characterization. The varying thicknesses of *m*-MTDATA (hole-transport/hole-injection layer) and PPT (electron-transport/hole-blocking layer) are associated with different roles for each of the materials in the different OLEDs. In device A, they provide only transport and injection of carriers to the emissive layer (bThBODIPY), while in device B they additionally take part in the formation of an exciplex state. The two devices differed only by the thickness of the bThBODIPY layer (70 nm in device A and 4 nm in device B). In device A the thickness of the bThBODIPY layer (70 nm) allowed only the emission from the exciton excited state of bThBODIPY, resulting in a strong electroluminescence band at 602 nm (Figure 6). This is due to the HOMO (HO-

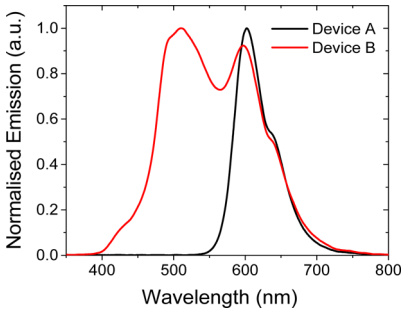

Figure 6. Electroluminescence spectra of devices A and B.

$MO_{m\text{-MTDATA}}$ is close to $HOMO_{bThBODIPY}$) and LUMO ($LUMO_{PPT}$ is close to $LUMO_{bThBODIPY}$) levels of the neighboring layers that facilitated the injection of holes and electrons in the emissive layer (Figure S7).[14] In device B, the reduced thickness of the bThBODIPY layer (4 nm) allowed exciplex formation between the layers of *m*-MTDATA and PPT.[47] The thickness of the emissive layer was less than the characteristic length associated with the exciplex wave function. This allowed the formation of a strong bound state between *m*-MTDATA and PPT layers with tunneling through the bThBODIPY spacer layer.[30] Consequently, the EL spectrum of device B had a more complex shape and contained three additional bands (λ_{max} = 428, 495, and 511 nm) (Figure 6). The band at 428 nm and the shoulder at 495 nm are due to the

DOI: 10.1021/acsami.6b13689
ACS Appl. Mater. Interfaces 2017, 9, 4750−4757

recombination of excitons and excimers in the *m*-MTDATA layer,[36] while the band centered at 511 nm is due to the well-known exciplex emission of the *m*-MTDATA:PPT couple.[10] The main characteristics of devices A and B are summarized in Table 1. Device A presented CIE 1931 coordinates (0.49, 0.42),

Table 1. Characteristics of Devices A and B

	device A	device B
V_{on} (V)	4	3
max brightness (cd m^{-2})	28829	6579
max current efficiency (cd A^{-1})	13.13	2.26
max power efficiency (lm W^{-1})	4.75	1.2
max external quantum efficiency (%)	6.8	1.17
CIE 1931 coordinates (*x*, *y*)	(0.49, 0.42)	(0.39, 0.35)

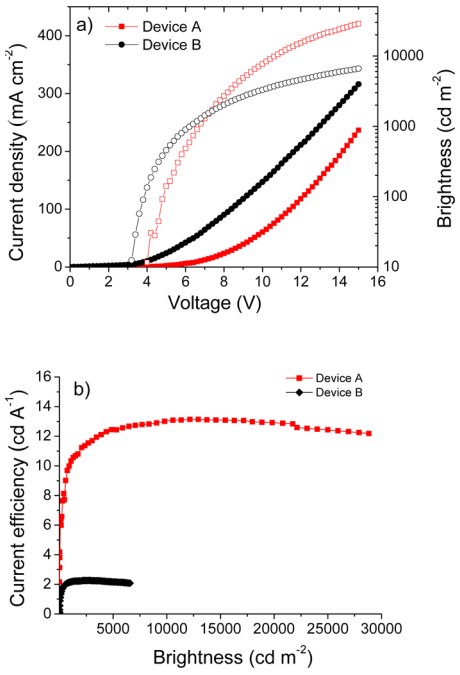

Figure 7. Current density–voltage and brightness–voltage (a) and current efficiency–current density (b) characteristics of devices A and B.

with high brightness (28829 cd m^{-2}) and efficiencies (Figure 7, Table 1, and Figure S8). These are due to the relatively high emission quantum yield of bThBODIPY in the solid state in combination with the efficient recombination of holes and electrons in the transport layers; this provides the background for an excellent balance between the electrons and holes in the bThBODIPY layer. A brightness of 6579 cd m^{-2} at 15 V with a current efficiency of 2.26 cd A^{-1} was recorded for device B. The CIE 1931 coordinates of (0.39, 0.35) are close to those of the calibrated white light (0.33, 0.33). The lower operating voltage of device B, when compared with device A, is due to the barrier-free exciplex emission[48] generated by electron tunneling from the PPT to the *m*-MTDATA layers.[49] At first glance device B seems far behind in external quantum efficiency (1.17%) (Table 1 and Figure 7) in comparison with the pure exciplex OLED based on PPT and *m*-MTDATA (10%).[10] However, in the pure exciplex device the efficiency drops to 0.4% at high brightness due to the efficiency roll-off. In contrast, device B is characterized by stable external quantum efficiency over a wide range of working current densities (30–315 mA cm^{-2}, Figure 7). The increased separation distance between the electrons and holes in the intermolecular state (PPT:*m*-MTDATA exciplex) by introduction of an ultrathin layer of bThBODIPY results in a reduction of the spin exchange energy of the exciplex state (Δ_{ST}) and therefore reduces the probability of triplet-polaron annihilation.[13,50] Thus, the roll-off efficiency at high current densities was improved, decreasing the Δ_{ST} and broadening the exciton formation width.[50]

High external quantum efficiency of the nonexciplex fluorescent device A can be explained by the advanced confinement of the hole and electron injection layers with the ambipolar bThBODIPY layer. Here, effective double injection and blocking of holes and electrons occur for the complete absence of barriers for both charge carriers at the *m*-MTDATA/bThBODIPY and bThBODIPY/PPT interfaces and for the high blocking barriers (1.2 eV) for both charge carriers. Another important advantage of device A is the *m*-MTDATA and PPT exciton confinement with bThBODIPY[51] since both *m*-MTDATA and PPT have a larger energy gap (3.1 eV for *m*-MTDATA and 3.7 eV for PPT) than bThBODIPY (2.3 eV) (Figure S7). As a result, the recombination zone is broadly distributed in the ambipolar bThBODIPY layer without exciton quenching of luminescence at the electrodes.[52]

bThBODIPY as a Dye for Optically Pumped Lasing in a Cholesteric Liquid Crystal. The fluorescence characteristics of bThBODIPY (Figure 2) suggest that it can be used for laser generation. There are many different approaches for the construction of dye lasers although all are based on the common principle of optical feedback resonant amplification. In commercially produced lasers the optical feedback is usually achieved with mirror resonators. Modern laser resonators are produced with high quality optical elements and require precision alignment, resulting in a bottleneck in production. Recently, significant effort has been focused on developing lasers utilizing mirrorless principles of optical feedback.[53,54] One of these mirrorless feedback mechanisms is selective light reflection in cholesteric liquid crystals (ChLC),[55] which under special conditions act as 1D photonic crystals.[56] Light emission from a fluorescent dye dissolved in cholesteric liquid crystals is inhibited within the spectral range of the photonic band gap (PhBG),[57] which is the selective reflection band for a ChLC, but leaks as strongly amplified laser radiation[58,59] at the PhBG edges. As such, highly effective fluorescent dyes for ChLC lasers are in great demand. On the other hand, modern trends to develop multiple-in-one microdevices set requirements for multifunctional active materials. In this context, the newly synthesized bThBODIPY dye, demonstrated above to be an effective material for WOLEDs, can be effectively used as a dye for a ChLC laser, possibly setting the basis for the development of compact and on-chip WOLED-pumped ChLC lasers.

We used two different experimental settings to achieve laser emission, which differ in the way the bThBODIPY dye (acting as the active element) and the ChLC (serving to provide the optical feedback) are combined. A first laser was obtained following a classical approach,[55] in which the dye was dissolved in a planar layer of ChLC. In the second setting, the dye was dissolved in an optically isotropic solvent; a flat capillary with this isotropic solution was sandwiched between two identical dye-free ChLC planar cells, serving as Bragg mirrors of resonation. The second setting, which to the best of our

DOI: 10.1021/acsami.6b13689
ACS Appl. Mater. Interfaces 2017, 9, 4750–4757

knowledge has never been reported before, will be referred hereinafter as "a sandwich capillary laser".

In order to have efficient laser generation, the cholesteric PhBG must be overlapped with the dye fluorescence emission band (DFEB). The spectral location of the PhBG of a cholesteric mixture is defined by the concentration of the chiral dopant in a liquid crystalline matrix. Figure 8 shows an overlap

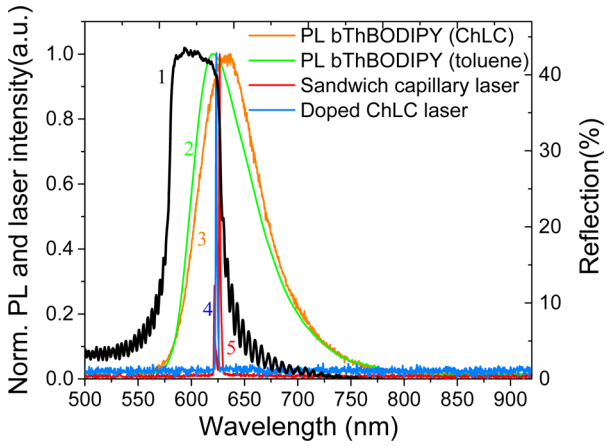

Figure 8. Fluorescence spectrum of the bThBODIPY dye in toluene (2) and in the ChLC (5), reflection spectrum of the ChLC cell (1), laser emission spectra from the flat dye-doped ChLC cell (4), and from capillary with dye solution in toluene (3), sandwiched between two dye-free ChLC cells.

of the cholesteric PhBG with the DFEB. Laser generation produced by the first setting, with the dye-doped cholesteric cell (Figure 9a and Figure S9), was registered (blue line in

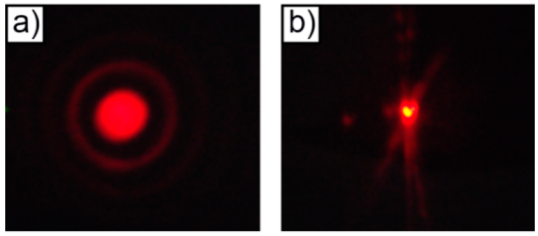

Figure 9. Photographs of laser emission patterns formed by (a) the doped ChLC cell and (b) capillary sandwich laser media.

Figure 8) at the long-wavelength edge of the cholesteric PhBG (black line in Figure 8), confirming its photonic nature. Lasing was stable for excitation energy values exceeding the threshold of ca. 0.6 μJ pulse^{-1} (Figure 10).

The laser emits in both the forward and backward directions, meaning that the true output lasing energy is double the value measured with the energy meter (in the forward direction), as shown in Figure 10. The second setting, based on the sandwich capillary approach described above, produces lasing similar to the classic case of ChLC doped with the dye. Excitation of the isotropic solution of dye with a laser beam at an incidence angle of 10°, focused inside the capillary, resulted in stable lasing (Figure 9b and Figure S9) at the long-wavelength edge of the cholesteric PhBG (red line in Figure 8).

The emission was close to that obtained in the dye-doped ChLC cell (blue line in Figure 8) and confirms that the lasing effect is photonic in nature, even though the dye is not dissolved in the ChLC. Stable lasing was registered for

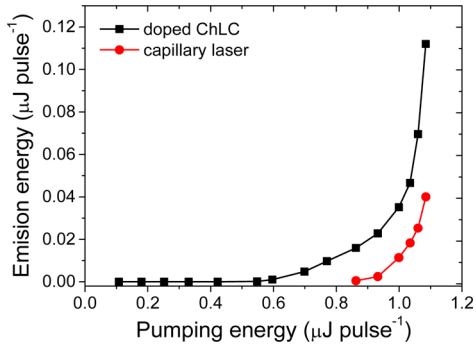

Figure 10. Laser emission energy as a function of the excitation energy for a dye-doped cholesteric cell (black squares) and capillary with dye solution (red stars) sandwiched between two dye-free cholesteric cells.

excitation energy values above 0.9 μJ pulse^{-1} (red line in Figure 10). This energy is considerably higher than the activation threshold for lasing in the dye-doped cell and is associated most probably with the loss of energy at the capillary interfaces. Additionally, there is a strong emission leak from the capillary ends. This means that the wave-guiding lasing modes take some part of the emission energy, thereby decreasing the output of the PhBG mode. Although the lasing energy activation threshold is higher for the capillary construction than for the conventional dye-doped cell, the capillary construction can be very convenient when the amount of emissive material is limited. Furthermore, the same capillary laser can be inserted between different pairs of ChLC cells that exhibit different PhBGs, leading to spectral shifts of the laser emission. Conversely, this new method allows for rapid screening of potential lasing materials through altering the capillary within the same pair of ChLC cells.

CONCLUSIONS

The new ambipolar red emissive compound bThBODIPY was synthesized, and the optical, photophysical, and electrochemical properties were studied. Hole and electron mobilities were estimated for bThBODIPY using the time-of-flight technique with values of 3.3×10^{-4} and 2×10^{-4} cm^2 V^{-1} s^{-1} (at electric fields higher than 5.3×10^5 V), respectively. The BODIPY derivative was used, first as a single emitting layer and then as a spacer, in the fabrication of two OLEDs. A new interface engineering method for the preparation of an efficient white OLED by embedding an ultrathin layer of bThBODIPY in the exciplex formation region (between layers of PPT and *m*-MTDATA) was developed. The resulting OLED displayed highly efficient exciplex and exciton emission simultaneously, resulting in white emission with CIE 1931 color coordinates (0.39, 0.35) close to those of calibrated white light. The WOLED achieved stable current efficiency over a wide range of working current densities with next to no efficiency roll-off. The bThBODIPY material was further employed as a ChLC laser dye. A new construction method in which a flat capillary filled with an optically isotropic dye solution is sandwiched between two dye-free planar ChLC cells was described. This provides optically pumped lasing at the same wavelength as in the classical scheme of a dye-doped planar ChLC cell. Facile assembly/disassembly of the capillary laser can be useful for optimization of laser characteristics using small amounts of dye and ChLCs; thus, it can be used as a simple method to explore new active laser media and to optimize the concentration dependencies of the lasing parameters.

DOI: 10.1021/acsami.6b13689
ACS Appl. Mater. Interfaces 2017, 9, 4750−4757

■ ASSOCIATED CONTENT

Supporting Information

The Supporting Information is available free of charge on the ACS Publications website at DOI: 10.1021/acsami.6b13689.

Experimental section, characterization of bTHBODIPY (^{1}H NMR, ^{13}C NMR, TGA, DFT calculation, photoelectron spectrum, and fluorescence decay curves of bThBODIPY for a vacuum-deposited film recorded at 605 and 650 nm), energy band diagram of devices, CIE 1931 chromaticity coordinates of OLEDs, and photographs of the laser devices (PDF)

■ AUTHOR INFORMATION

Corresponding Authors

*E-mail olavrent@kent.edu (O.D.L.).
*E-mail peter.skabara@strath.ac.uk (P.J.S.).

ORCID

Peter J. Skabara: 0000-0001-7319-0464

Notes

The authors declare no competing financial interest.

■ ACKNOWLEDGMENTS

The authors thank the European Commission (Marie Curie Action of FP7, Grant No.: PIRSES-GA-2013-612670), the UK Engineering and Physical Sciences Research Council (Grant No.: EP/I012591/1), the University of Strathclyde, and the Kaunas University of Technology for financial support. P.J.S. thanks the Royal Society for a Wolfson Research Merit Award. M.C. is grateful for financial support from grant 674990 EXCILIGHT-H2020-MSCA-ITN-2015. O.D.L. acknowledges support from NSF grant DMR-1410378 for studies of the lasing effect. The data associated with this research are available at http://dx.doi.org/10.15129/dd4e4a3b-71a9-4cd2-a640-61b8ab54eead or from the corresponding author.

■ REFERENCES

(1) Yan, F.; Xing, G.; Chen, R.; Demir, H. V.; Sun, H.; Sum, T. C.; Sun, X. W. Efficient Three-Color White Organic Light-Emitting Diodes with a Spaced Multilayer Emitting Structure. *Appl. Phys. Lett.* **2015**, *106*, 023302.

(2) Ding, L.; Dong, S.-C.; Jiang, Z.-Q.; Chen, H.; Liao, L.-S. Orthogonal Molecular Structure for Better Host Material in Blue Phosphorescence and Larger OLED White Lighting Panel. *Adv. Funct. Mater.* **2015**, *25*, 645−650.

(3) Park, J. W.; Shin, D. C.; Park, S. H. Large-Area OLED Lightings and Their Applications. *Semicond. Sci. Technol.* **2011**, *26*, 034002.

(4) Lai, C.-C.; Huang, M.-J.; Chou, H.-H.; Liao, C.-Y.; Rajamalli, P.; Cheng, C.-H. M -Indolocarbazole Derivative as a Universal Host Material for RGB and White Phosphorescent OLEDs. *Adv. Funct. Mater.* **2015**, *25*, 5548−5556.

(5) Lee, J.; Chen, H.-F.; Batagoda, T.; Coburn, C.; Djurovich, P. I.; Thompson, M. E.; Forrest, S. R. Deep Blue Phosphorescent Organic Light-Emitting Diodes with Very High Brightness and Efficiency. *Nat. Mater.* **2015**, *15*, 92−98.

(6) Zhao, Y.; Chen, J.; Ma, D. Ultrathin Nondoped Emissive Layers for Efficient and Simple Monochrome and White Organic Light-Emitting Diodes. *ACS Appl. Mater. Interfaces* **2013**, *5*, 965−971.

(7) Su, S.-J.; Gonmori, E.; Sasabe, H.; Kido, J. Highly Efficient Organic Blue-and White-Light-Emitting Devices Having a Carrier- and Exciton-Confining Structure for Reduced Efficiency Roll-Off. *Adv. Mater.* **2008**, *20*, 4189−4194.

(8) Angioni, E.; Chapran, M.; Ivaniuk, K.; Kostiv, N.; Cherpak, V.; Stakhira, P.; Lazauskas, A.; Tamulevičius, S.; Volyniuk, D.; Findlay, N. J.; Tuttle, T.; Grazulevicius, J. V.; Skabara, P. J. A Single Emitting Layer White OLED Based on Exciplex Interface Emission. *J. Mater. Chem. C* **2016**, *4*, 3851−3856.

(9) Michaleviciute, A.; Gurskyte, E.; Volyniuk, D. Y.; Cherpak, V. V.; Sini, G.; Stakhira, P. Y.; Grazulevicius, J. V. Star-Shaped Carbazole Derivatives for Bilayer White Organic Light-Emitting Diodes Combining Emission from Both Excitons and Exciplexes. *J. Phys. Chem. C* **2012**, *116*, 20769−20778.

(10) Goushi, K.; Adachi, C. Efficient Organic Light-Emitting Diodes through up-Conversion from Triplet to Singlet Excited States of Exciplexes. *Appl. Phys. Lett.* **2012**, *101*, 023306.

(11) Hung, W.-Y.; Fang, G.-C.; Lin, S.-W.; Cheng, S.-H.; Wong, K.-T.; Kuo, T.-Y.; Chou, P.-T. The First Tandem, All-Exciplex-Based WOLED. *Sci. Rep.* **2014**, *4*, 5161.

(12) Hirata, S.; Sakai, Y.; Masui, K.; Tanaka, H.; Lee, S. Y.; Nomura, H.; Nakamura, N.; Yasumatsu, M.; Nakanotani, H.; Zhang, Q.; Shizu, K.; Miyazaki, H.; Adachi, C. Highly Efficient Blue Electroluminescence Based on Thermally Activated Delayed Fluorescence. *Nat. Mater.* **2014**, *14*, 330−336.

(13) Chen, P.; Peng, Q.; Yao, L.; Gao, N.; Li, F. Identifying the Efficient Inter-Conversion between Singlet and Triplet Charge-Transfer States by Magneto-Electroluminescence Study. *Appl. Phys. Lett.* **2013**, *102*, 063301.

(14) Hung, W.-Y.; Chiang, P.-Y.; Lin, S.-W.; Tang, W.-C.; Chen, Y.-T.; Liu, S.-H.; Chou, P.-T.; Hung, Y.-T.; Wong, K.-T. Balance the Carrier Mobility To Achieve High Performance Exciplex OLED Using a Triazine-Based Acceptor. *ACS Appl. Mater. Interfaces* **2016**, *8*, 4811−4818.

(15) Lee, J.-H.; Cheng, S.-H.; Yoo, S.-J.; Shin, H.; Chang, J.-H.; Wu, C.-I.; Wong, K.-T.; Kim, J.-J. An Exciplex Forming Host for Highly Efficient Blue Organic Light Emitting Diodes with Low Driving Voltage. *Adv. Funct. Mater.* **2015**, *25*, 361−366.

(16) Nakanotani, H.; Furukawa, T.; Morimoto, K.; Adachi, C. Long-Range Coupling of Electron-Hole Pairs in Spatially Separated Organic Donor-Acceptor Layers. *Sci. Adv.* **2016**, *2*, e1501470−e1501470.

(17) Shah, M.; Thangaraj, K.; Soong, M.-L.; Wolford, L. T.; Boyer, J. H.; Politzer, I. R.; Pavlopoulos, T. G. Pyrromethene-BF2 Complexes as Laser dyes:1. *Heteroat. Chem.* **1990**, *1*, 389−399.

(18) Boyer, J. H.; Haag, A. M.; Sathyamoorthi, G.; Soong, M.-L.; Thangaraj, K.; Pavlopoulos, T. G. Pyrromethene-BF2 Complexes as Laser Dyes: 2. *Heteroat. Chem.* **1993**, *4*, 39−49.

(19) Sajjad, M. T.; Manousiadis, P. P.; Orofino, C.; Cortizo-Lacalle, D.; Kanibolotsky, A. L.; Rajbhandari, S.; Amarasinghe, D.; Chun, H.; Faulkner, G.; O'Brien, D. C.; Skabara, P. J.; Turnbull, G. A.; Samuel, I. D. W. Fluorescent Red-Emitting BODIPY Oligofluorene Star-Shaped Molecules as a Color Converter Material for Visible Light Communications. *Adv. Opt. Mater.* **2015**, *3*, 536−540.

(20) Ulrich, G.; Ziessel, R.; Harriman, A. The Chemistry of Fluorescent Bodipy Dyes: Versatility Unsurpassed. *Angew. Chem., Int. Ed.* **2008**, *47*, 1184−1201.

(21) Bonardi, L.; Kanaan, H.; Camerel, F.; Jolinat, P.; Retailleau, P.; Ziessel, R. Fine-Tuning of Yellow or Red Photo- and Electroluminescence of Functional Difluoro-Boradiazaindacene Films. *Adv. Funct. Mater.* **2008**, *18*, 401−413.

(22) Zhang, D.; Wen, Y.; Xiao, Y.; Yu, G.; Liu, Y.; Qian, X. Bulky 4-Tritylphenylethynyl Substituted Boradiazaindacene: Pure Red Emission, Relatively Large Stokes Shift and Inhibition of Self-Quenching. *Chem. Commun.* **2008**, *39*, 4777.

(23) Vu, T. T.; Badré, S.; Dumas-Verdes, C.; Vachon, J.-J.; Julien, C.; Audebert, P.; Senotrusova, E. Y.; Schmidt, E. Y.; Trofimov, B. A.; Pansu, R. B.; Clavier, G.; Méallet-Renault, R. New Hindered BODIPY Derivatives: Solution and Amorphous State Fluorescence Properties. *J. Phys. Chem. C* **2009**, *113*, 11844−11855.

(24) Ozdemir, T.; Atilgan, S.; Kutuk, I.; Yildirim, L. T.; Tulek, A.; Bayindir, M.; Akkaya, E. U. Solid-State Emissive BODIPY Dyes with Bulky Substituents As Spacers. *Org. Lett.* **2009**, *11*, 2105−2107.

(25) Kubota, Y.; Uehara, J.; Funabiki, K.; Ebihara, M.; Matsui, M. Strategy for the Increasing the Solid-State Fluorescence Intensity of pyrromethene−BF2 Complexes. *Tetrahedron Lett.* **2010**, *51*, 6195−6198.

DOI: 10.1021/acsami.6b13689
ACS Appl. Mater. Interfaces 2017, 9, 4750−4757

(26) Xi, H.; Yuan, C.-X.; Li, Y.-X.; Liu, Y.; Tao, X.-T. Crystal Structures and Solid-State Fluorescence of BODIPY Dyes Based on Λ-Shaped Tröger's Base. *CrystEngComm* **2012**, *14*, 2087.
(27) Loudet, A.; Burgess, K. BODIPY Dyes and Their Derivatives: Syntheses and Spectroscopic Properties. *Chem. Rev.* **2007**, *107*, 4891−4932.
(28) Chong, H.; Lin, H.-A.; Shen, M.-Y.; Liu, C.-Y.; Zhao, H.; Yu, H. Step-Economical Syntheses of Functional BODIPY-EDOT π-Conjugated Materials through Direct C−H Arylation. *Org. Lett.* **2015**, *17*, 3198−3201.
(29) Bonnier, C.; Machin, D. D.; Abdi, O.; Koivisto, B. D. Manipulating Non-Innocent π-Spacers: The Challenges of Using 2,6-Disubstituted BODIPY Cores within Donor−acceptor Light-Harvesting Motifs. *Org. Biomol. Chem.* **2013**, *11*, 3756−3760.
(30) Yin, S.; Nie, W.; Mohite, A. D.; Saxena, A.; Smith, D. L.; Ruden, P. P. Current−voltage Characteristics of Organic Heterostructure Devices with Insulating Spacer Layers. *Org. Electron.* **2015**, *24*, 26−29.
(31) Kohary, K. Exciplex Kinetics in Nanocrystal Organic Light-Emitting Diodes. *J. Mater. Sci.: Mater. Electron.* **2009**, *20*, 10−14.
(32) Wu, Q.; Zhang, T.; Peng, Q.; Wang, D.; Shuai, Z. Aggregation Induced Blue-Shifted Emission − the Molecular Picture from a QM/MM Study. *Phys. Chem. Chem. Phys.* **2014**, *16*, 5545.
(33) Chen, Y.; Zhao, J.; Guo, H.; Xie, L. Geometry Relaxation-Induced Large Stokes Shift in Red-Emitting Borondipyrromethenes (BODIPY) and Applications in Fluorescent Thiol Probes. *J. Org. Chem.* **2012**, *77*, 2192−2206.
(34) Lakowicz, J. R., Ed.; *Principles of Fluorescence Spectroscopy*, 3rd ed.; Springer: Boston, MA, 2006.
(35) Mitani, T.; Yamanaka, T.; Suzui, M.; Horigome, T.; Hayakawa, K.; Yamazaki, I. Time-Resolved Synchrotron Spectroscopy of Exciton Fluorescence in Anthracene Single Crystals. *J. Lumin.* **1988**, *39*, 313−322.
(36) Kalinowski, J. Excimers and Exciplexes in Organic Electroluminescence. *Mater. Sci.* **2009**, *27*, 735−756.
(37) Improta, R.; Barone, V.; Scalmani, G.; Frisch, M. J. A State-Specific Polarizable Continuum Model Time Dependent Density Functional Theory Method for Excited State Calculations in Solution. *J. Chem. Phys.* **2006**, *125*, 054103.
(38) Furche, F.; Ahlrichs, R. Adiabatic Time-Dependent Density Functional Methods for Excited State Properties. *J. Chem. Phys.* **2002**, *117*, 7433.
(39) Frisch, M. J.; Trucks, G. W.; Schlegel, H. B.; Scuseria, G. E.; Robb, M. A.; Cheeseman, J. R.; Scalmani, G.; Barone, V.; Mennucci, B.; Petersson, G. A.; Nakatsuji, H.; Caricato, M.; Li, X.; Hratchian, H. P.; Izmaylov, A. F.; Bloino, J.; Zheng, G.; Sonnenberg, J. L.; Hada, M.; Ehara, M.; Toyota, K.; Fukuda, R.; Hasegawa, J.; Ishida, M.; Nakajima, T.; Honda, Y.; Kitao, O.; Nakai, H.; Vreven, T.; Montgomery, Jr., J. A.; Peralta, J. E.; Ogliaro, F.; Bearpark, M.; Heyd, J. J.; Brothers, E.; Kudin, K. N.; Staroverov, V. N.; Kobayashi, R.; Normand, J.; Raghavachari, K.; Rendell, A.; Burant, J. C.; Iyengar, S. S.; Tomasi, J.; Cossi, M.; Rega, N.; Millam, J. M.; Klene, M.; Knox, J. E.; Cross, J. B.; Bakken, V.; Adamo, C.; Jaramillo, J.; Gomperts, R.; Stratmann, R. E.; Yazyev, O.; Austin, A. J.; Cammi, R.; Pomelli, C.; Ochterski, J. W.; Martin, R. L.; Morokuma, K.; Zakrzewski, V. G.; Voth, G. A.; Salvador, P.; Dannenberg, J. J.; Dapprich, S.; Daniels, A. D.; Farkas, O.; Foresman, J. B.; Ortiz, J. V; Cioslowski, J.; Fox, D. J. Gaussian, Inc.: Wallingford, CT, 2009.
(40) Nepomnyashchii, A. B.; Bröring, M.; Ahrens, J.; Bard, A. J. Synthesis, Photophysical, Electrochemical, and Electrogenerated Chemiluminescence Studies. Multiple Sequential Electron Transfers in BODIPY Monomers, Dimers, Trimers, and Polymer. *J. Am. Chem. Soc.* **2011**, *133*, 8633−8645.
(41) Findlay, N. J.; Orofino-Peña, C.; Bruckbauer, J.; Elmasly, S. E. T.; Arumugam, S.; Inigo, A. R.; Kanibolotsky, A. L.; Martin, R. W.; Skabara, P. J. Linear Oligofluorene-BODIPY Structures for Fluorescence Applications. *J. Mater. Chem. C* **2013**, *1*, 2249−2256.
(42) Ziessel, R.; Goze, C.; Ulrich, G.; Césario, M.; Retailleau, P.; Harriman, A.; Rostron, J. P. Intramolecular Energy Transfer in Pyrene−Bodipy Molecular Dyads and Triads. *Chem. - Eur. J.* **2005**, *11*, 7366−7378.
(43) Tse, S.; Cheung, C.; So, S. Charge Transport and Injection in Amorphous Organic Semiconductors. In *Organic Electronics*; CRC Press: 2009; pp 61−109.
(44) Borsenberger, P. M.; Shi, J. Hole Transport in a Vapor Deposited Phenylenediamine Molecular Glass. *Phys. Status Solidi B* **1995**, *191*, 461−469.
(45) Bučinskas, A.; Volyniuk, D.; Danyliv, Y.; Grazulevicius, J. V.; Baryshnikov, G.; Minaev, B.; Ivaniuk, K.; Cherpak, V.; Stakhira, P. N-Annelated Perylenes as Effective Green Emitters for OLEDs. *RSC Adv.* **2015**, *5*, 78150−78159.
(46) Stakhira, P.; Cherpak, V.; Volynyuk, D.; Ivastchyshyn, F.; Hotra, Z.; Tataryn, V.; Luka, G. Characteristics of Organic Light Emitting Diodes with Copper Iodide as Injection Layer. *Thin Solid Films* **2010**, *518*, 7016−7018.
(47) Graves, D.; Jankus, V.; Dias, F. B.; Monkman, A. Photophysical Investigation of the Thermally Activated Delayed Emission from Films of M-MTDATA:PBD Exciplex. *Adv. Funct. Mater.* **2014**, *24*, 2343−2351.
(48) Morteani, A. C.; Dhoot, A. S.; Kim, J.-S.; Silva, C.; Greenham, N. C.; Murphy, C.; Moons, E.; Ciná, S.; Burroughes, J. H.; Friend, R. H. Barrier-Free Electron−Hole Capture in Polymer Blend Heterojunction Light-Emitting Diodes. *Adv. Mater.* **2003**, *15*, 1708−1712.
(49) Park, T. J.; Lee, Y. K.; Kwon, S. K.; Kwon, J. H.; Jang, J. Resonant Tunneling Diode Made of Organic Semiconductor Superlattice. *Appl. Phys. Lett.* **2006**, *89*, 151114.
(50) Endo, A.; Sato, K.; Yoshimura, K.; Kai, T.; Kawada, A.; Miyazaki, H.; Adachi, C. Efficient up-Conversion of Triplet Excitons into a Singlet State and Its Application for Organic Light Emitting Diodes. *Appl. Phys. Lett.* **2011**, *98*, 083302.
(51) Wu, C.-C.; Lin, Y.-T.; Wong, K.-T.; Chen, R.-T.; Chien, Y.-Y. Efficient Organic Blue-Light-Emitting Devices with Double Confinement on Terfluorenes with Ambipolar Carrier Transport Properties. *Adv. Mater.* **2004**, *16*, 61−65.
(52) Kalinowski, J.; Mężyk, J.; Meinardi, F.; Tubino, R.; Cocchi, M.; Virgili, D. Exciton Quenching in Emitter Blends for Organic Light Emitting Devices Probed by Electric Field−dependent Time-Resolved Luminescence. *J. Chem. Phys.* **2008**, *128*, 124712.
(53) Nastishin, Y. A.; Dudok, T. H. Optically Pumped Mirrorless Lasing. A Review. Part I. Random Lasing. *Ukr. J. Phys. Opt.* **2013**, *14*, 146−170.
(54) Dudok, T. H.; Nastishin, Y. A. Optically Pumped Mirrorless Lasing. A Review. Part II. Lasing in Photonic Crystals and Microcavities. *Ukr. J. Phys. Opt.* **2014**, *15*, 47−67.
(55) de Gennes, P. G.; Prost, J. *The Physics of Liquid Crystals*, 2nd ed.; Clarendon: Oxford, 1995.
(56) Kopp, V. I.; Fan, B.; Vithana, H. K. M.; Genack, A. Z. Low-Threshold Lasing at the Edge of a Photonic Stop Band in Cholesteric Liquid Crystals. *Opt. Lett.* **1998**, *23*, 1707−1709.
(57) Yablonovitch, E. Inhibited Spontaneous Emission in Solid-State Physics and Electronics. *Phys. Rev. Lett.* **1987**, *58*, 2059−2062.
(58) Ilchishin, I. P.; Tikhonov, E. A.; Tishchenko, V. G.; Shpak, M. T. Generation of a Tunable Radiation by Impurity Cholesteric Liquid Crystals. *JETP Lett.* **1980**, *32*, 24−27.
(59) Palffy-Muhoray, P.; Cao, W.; Moreira, M.; Taheri, B.; Munoz, A. Photonics and Lasing in Liquid Crystal Materials. *Philos. Trans. R. Soc., A* **2006**, *364*, 2747−2761.

DOI: 10.1021/acsami.6b13689
ACS Appl. Mater. Interfaces 2017, 9, 4750−4757

Supporting Information

An ambipolar BODIPY derivative for a white exciplex OLED and cholesteric liquid crystal laser toward multi-functional devices

Marian Chapran,[1,2] Enrico Angioni,[3] Neil J. Findlay,[3] Benjamin Breig,[3] Vladyslav Cherpak,[4] Pavlo Stakhira,[2] Tell Tuttle,[3] Dmytro Volyniuk,[5] Juozas V. Grazulevicius,[5] Yuriy A. Nastishin,[4] Oleg D. Lavrentovich,*[4] and Peter J. Skabara*[3]

[1] Lodz University of Technology, Department of Molecular Physics, Zeromskiego 116, 90-924 Lodz, Poland
[2] Lviv Polytechnic National University, S. Bandera 12, 79013 Lviv, Ukraine
[3] WestCHEM, Department of Pure and Applied Chemistry, University of Strathclyde, Glasgow, G1 1XL, UK
[4] Liquid Crystal Institute and Chemical Physics Interdisciplinary Program, Kent State University, Kent, Ohio 44242, USA
[5] Department of Polymer Chemistry and Technology, Kaunas University of Technology, Radvilenu Plentas 19, LT-50254 Kaunas, Lithuania

*olavrent@kent.edu
*peter.skabara@strath.ac.uk

Contents

Experimental section

Materials. All reactions were performed using vacuum Schlenk lines, in an inert atmosphere of nitrogen. Dry solvents were obtained from a solvent purification system (SPS 400 from Innovative Technologies) using alumina as the drying agent. The compounds tetrakis(triphenylphosphine)palladium(0)[1], 4,4-di-fluoro-1,3,5,7,8-pentamethyl-4-bora-3a,4a-diaza-s-indacene[2], 4,4-di-fluoro-2,6-diiodo-1,3,5,7,8-pentamethyl-4-bora-3a,4a-diaza-s-indacene[3] and 4(-hexylthiopen-2-yl) trimethylstannane[4] were obtained and analyzed using literature procedures. All the other reagents were purchased from Sigma Aldrich or Alfa Aesar and used without further purification.

4,4-Di-fluoro-2,6-di(4-hexylthiopen-2-yl)-1,3,5,7,8-pentamethyl-4-bora-3a,4a-diaza-s-indacene (bThBODIPY). 4,4-di-fluoro-2,6-diiodo-1,3,5,7,8-pentamethyl-4-bora-3a,4a-diaza-s-indacene (350 mg, 0.68 mmol) and 4(-hexylthiopen-2-yl) trimethylstannane (0.627 g, 1.70 mmol) were dissolved in dry toluene (40 mL) under nitrogen. Tetrakis(triphenylphosphine)palladium(0) (0.228g, 0.14 mmol) was added and the resultant reaction mixture was stirred and heated to reflux for 20 h. The reaction was cooled to room temperature and an additional portion of tetrakis(triphenylphosphine)palladium(0) was added (0.114 g, 0.07 mmol). The mixture was stirred and heated at reflux for 24 h. The mixture was diluted with water (100mL) and the organic phase was extracted with CH_2Cl_2 (3 × 50 mL). The combined organic layers were washed with water (3 × 100 mL), dried over $MgSO_4$, filtered and concentrated under reduced pressure. Purification by column chromatography on silica gel eluting with 60% hexane in dichloromethane afforded the title compound as a deep red powder (0.138 g, yield 34%). ^{1}H NMR (400 MHz, $CDCl_3$) δ 6.97 (d, *J* = 1.2 Hz, 2H, Ar-H), 6.74 (d, *J* = 1.4 Hz, 2H, Ar-H), 2.70 (s, 3H, CH_3), 2.64 (t, 4H, *J* = 7.7 Hz, CH_2), 2.56 (s, 6H, CH_3), 2.43 (s, 6H, CH_3), 1.66 (q, *J* = 7.6, 7.1Hz, 4H, CH_2), 1.34 – 1.32 (m, 12H, CH_2), 0.92 (t, *J* = 6.9 Hz, 6H, CH_2); ^{13}C NMR (101 MHz, $CDCl_3$) δ 153.6, 143.7, 142.2, 138.6, 134.2, 132.3, 129.6, 126.8, 120.8, 31.8, 30.7, 30.6, 29.2, 22.8, 17.5, 15.8, 14.2, 13.5; MS (MALDI-TOF) *m/z* calcd for $C_{34}H_{45}BF_2N_2S_2$: 594.31; found, 594.30; Elemental analysis calcd for $C_{34}H_{45}BF_2N_2S_2$: C 68.67, H 7.63, N 4.71%; found: C 68.54, H 7.46, N 4.59%; TGA: 5% mass loss at 326°C, 10% mass loss at 342°C; Melting Point: 132-133°C.

Methods. ^{1}H and ^{13}C NMR spectra were recorded on a Bruker AVR 400 NMR spectrometer using $CDCl_3$ as the solvent. Chemical shifts are given in ppm using the residual solvent signal ($CDCl_3$) as internal reference and coupling constants (J) in Hz. Column chromatography and TLC were performed on silica gel 60 (230-400 mesh, Merck) and silica gel (60) F254 plates (Merck) respectively. Thermogravimetric analysis (TGA) was performed using a Perkin-Elmer Thermogravimetric Analyzer TGA7 under a constant flow of argon. Melting points were measured using a Stuart Scientific melting point apparatus. The target compound was characterized by matrix-assisted laser desorption/ionisation time-of-flight (MALDI-TOF) using a Shimadzu Biotech Axima Curved Field Reflectron mass spectrometer. Elemental analysis was performed on a Perkin Elmer 2400 elemental analyzer. Cyclic voltammetry (CV) measurements were performed on a CH Instruments 660A electrochemical workstation with iR compensation using anhydrous dichloromethane as the solvent and tetrabutylammonium hexafluorophosphate as the electrolyte (concentration 0.1 M). The electrodes used were glassy carbon, platinum wire and silver wire as the working, counter and reference electrodes, respectively. All solutions were degassed using Ar and contained the analyte at concentrations of ca. 10^{-4} M. All measurements were referenced against the E1/2 of the Fc/F c+ redox couple and HOMO and LUMO energy levels were referenced to ferrocene, which has a HOMO of −4.8 eV.[5] Photoluminescence measurements were performed with a Jasco FP-6500 fluorimeter using dichloromethane solution of the analyte (10^{-5} M). Absorption spectra were recorded with a Shimadzu UV-2700 spectrophotometer. Photoluminescence and absorption spectra of thin films prepared by vacuum deposition technique were recorded at room temperature with Edinburgh Instruments FLS980 and PerkinElmer Lambda 25 spectrometers, respectively. Absolute photoluminescence quantum yield (PLQY) measurements were performed using a calibrated integrating sphere attached to an Ocean Optics USB2000+ spectrometer and a Gooch & Housego double monochromator with a quartz halogen lamp. The ionisation potential of **bThBODIPY** was measured by the electron photoemission method in air.[6] The samples were fabricated by means of vacuum deposition of **bThBODIPY** at 10^{-6} Torr onto fluorine doped tin oxide coated glass substrates. The experimental setup consisted of a deep-UV deuterium light source ASBN-D130-CM, a CM110 1/8m monochromator, a 6517B Keithley electrometer and was similar to that which was previously described.[7] The time of flight (TOF) technique was used for the estimation of the charge-transporting properties of **bThBODIPY**. The samples for TOF measurements were prepared by depositing thick layers (5.3 μm) of **bThBODIPY** by vacuum deposition on pre-cleaned glass/indium tin oxide (ITO) substrates, using aluminium as the top electrode. The TOF experiments were performed as described previously.[8] The TOF setup included a pulsed Nd:YAG laser (EKSPLA NL300, wavelength of 355 nm with a pulse of duration 3-6 ns), a Keithley 6517B electrometer and a Tektronix TDS 3052C oscilloscope. The thicknesses of thin films have been controlled during thermal vacuum evaporation using a frequency quartz sensor. This was previously calibrated for organic semiconductors materials by Bruker Dektak XT profilometer. The density–voltage and luminance–voltage dependences were measured using a semiconductor parameter analyzer HP 4145A. The measurement of brightness was obtained using a calibrated photodiode.[9,10] The electroluminescence spectrum was recorded with an Ocean Optics USB2000 spectrometer.

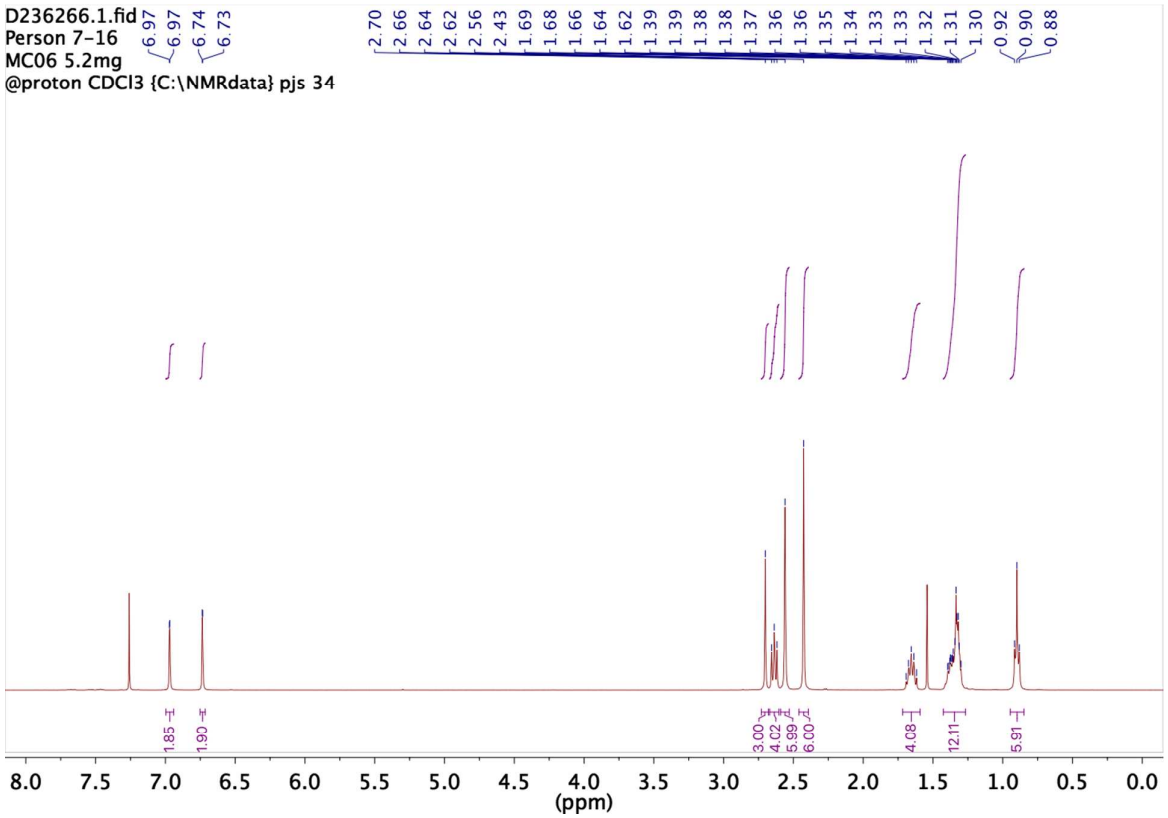

Figure S1 [1]H-NMR spectrum of **bThBODIPY** recorded in deuterated chloroform.

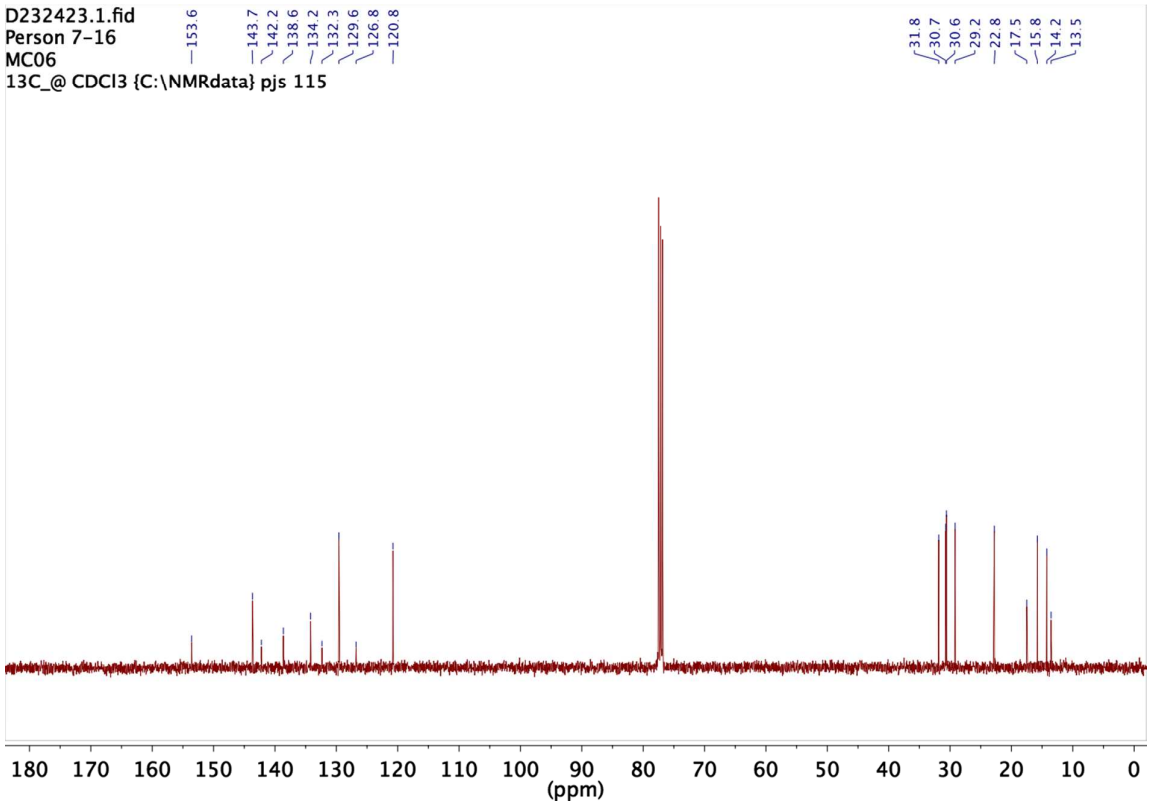

Figure S2 [13]C-NMR spectrum of bThBODIPY recorded in deuterated chloroform.

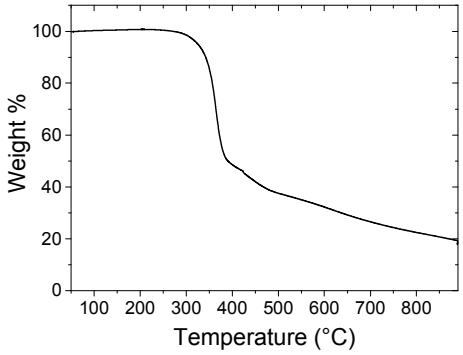

Figure S3 Thermogravimetric analyses of **bThBODIPY** in Argon (100-890°C).

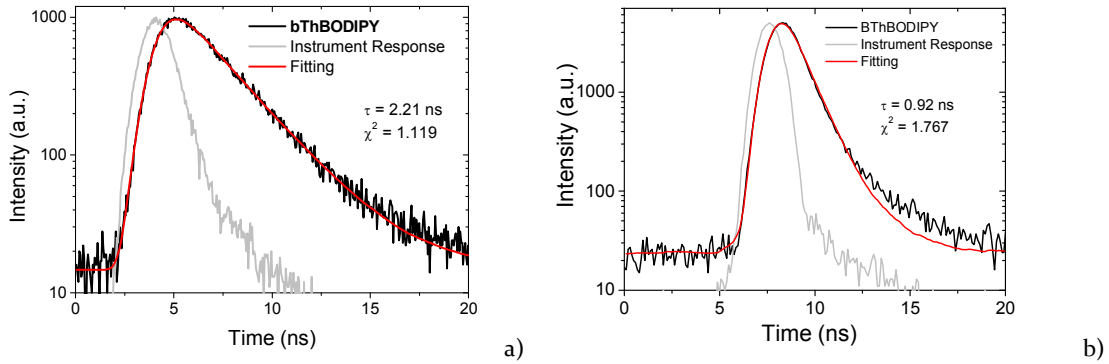

a) b)

Figure S4 Fluorescence decay curve of **bThBODIPY** for a vacuum deposited film recorded at 605 nm (a) and 650 nm (b).

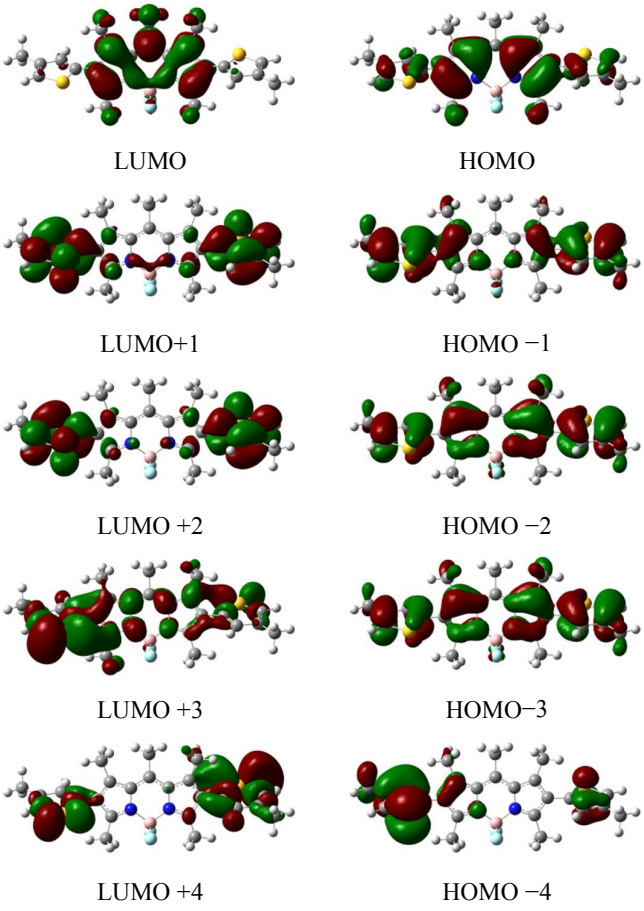

Figure S5 Energy diagram for the last ten occupied and first ten unoccupied molecular orbitals calculated at the B3LYP/6-311G (d,p) level of theory (left). Graphical representation of the last five occupied (HOMO to HOMO−4) and first five unoccupied (LUMO to LUMO+4) molecular orbitals (isosurfaces 0.020) calculated at the B3LYP/6-311G (d,p) level of theory (center and right) for **bThBODIPY**.

Table S1 Energies for the last five occupied and first five unoccupied molecular orbitals calculated at the B3LYP/6-311G (d,p) level of theory for **bThBODIPY**.

Orbital	Energy (eV)
124	0.46
123	0.35
122	-0.55
121	-0.60
LUMO	-2.67
HOMO	-5.60
118	-6.27
117	-6.30
116	-6.76
115	-6.80

Table S2 Wavelengths, energies, oscillator strengths and orbital assignments for the first 20 singlet vertical electronic transitions for **bThBODIPY** (vacuum) calculated at the B3LYP/6-311G (d,p) level of theory.

Wavelength (nm)	Energy (eV)	Oscillation Strength	Major contributions
453.3	2.73	0.5631	H-2->LUMO (15%), HOMO->LUMO (84%)
401.0	3.09	0.0157	H-1->LUMO (98%)
385.0	3.22	0.3621	H-2->LUMO (84%), HOMO->LUMO (16%)
347.3	3.57	0.0148	H-3->LUMO (93%)
343.0	3.62	0.0032	H-4->LUMO (98%)
333.6	3.72	0.0117	H-5->LUMO (92%)
323.5	3.83	0.0096	H-6->LUMO (98%)
278.0	4.46	0.0792	HOMO->L+1 (98%)
274.9	4.51	0.0005	HOMO->L+2 (96%)
261.3	4.74	0.0957	H-7->LUMO (87%)
239.9	5.17	0.3142	H-2->L+1 (57%), H-1->L+2 (26%)
238.3	5.20	0.0123	H-2->L+2 (36%), H-1->L+1 (45%)
233.8	5.30	0.001	H-8->LUMO (98%)
230.7	5.37	0.0419	HOMO->L+3 (67%), HOMO->L+5 (10%)
229.5	5.40	0.0017	H-2->L+2 (51%), H-1->L+1 (42%)
229.0	5.41	0.0019	H-2->L+1 (28%), H-1->L+2 (49%), HOMO->L+4 (15%)
229.0	5.41	0.0059	H-1->L+2 (14%), HOMO->L+4 (59%)
228.8	5.42	0.0596	H-3->L+1 (43%), H-3->L+2 (23%)
226.2	5.48	0.0153	H-4->L+1 (39%), H-4->L+2 (19%), H-3->L+2 (13%)
222.9	5.56	0.0667	H-2->L+3 (10%), H-1->L+4 (13%), HOMO->L+3 (21%), HOMO->L+5 (25%)

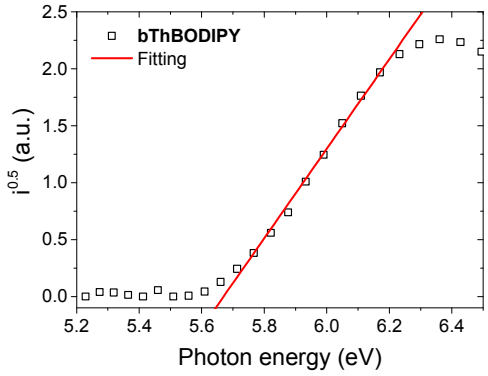

Figure S6. Photoelectron spectrum of the vacuum deposited film of bThBODIPY.

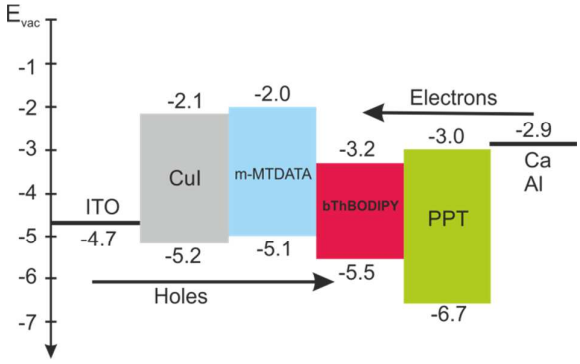

Figure S7 Energy level diagram of HOMO and LUMO levels (relative to vacuum level) for materials investigated in this work.

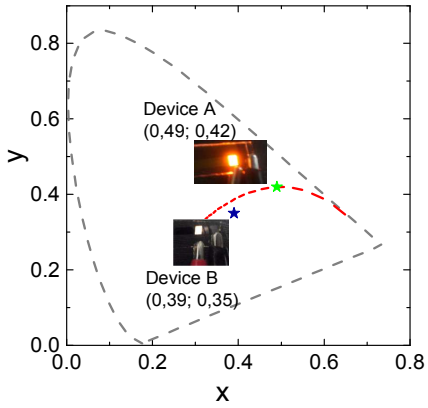

Figure S8 CIE 1931 chromaticity coordinates of devices A and B. The enclosed pictures represent devices A and B under operation conditions.

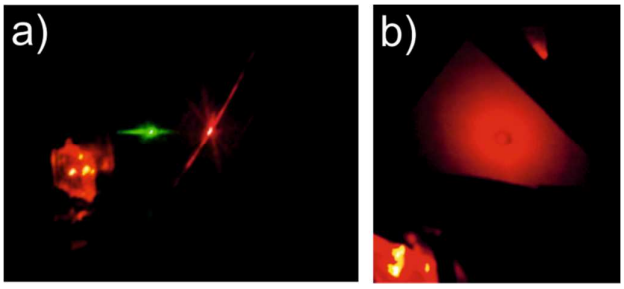

Figure S9 Photographs of the laser devices: capillary laser (a) and doped laser(b).

References

(1) Malatesia, L.; Angoletta, M. 231. Palladium(0) Compounds. Part II. Compounds with Triarylphosphines, Triaryl Phosphites, and Triarylarsines. *J. Chem. Soc.* **1957**, 1186.
(2) Guo, B.; Peng, X.; Cui, A.; Wu, Y.; Tian, M.; Zhang, L.; Chen, X.; Gao, Y. Synthesis and Spectral Properties of New Boron Dipyrromethene Dyes. *Dyes Pigm.* **2007**, *73*, 206–210.
(3) Bonardi, L.; Ulrich, G.; Ziessel, R. Tailoring the Properties of Boron−Dipyrromethene Dyes with Acetylenic Functions at the 2,6,8 and 4-B Substitution Positions. *Org. Lett.* **2008**, *10*, 2183–2186.
(4) Barbarella, G.; Bongini, A.; Zambianchi, M. Regiochemistry and Conformation of Poly(3-

Hexylthiophene) via the Synthesis and the Spectroscopic Characterization of the Model Configurational Triads. *Macromolecules* **1994**, *27*, 3039–3045.
(5) Bredas, J. L.; Silbey, R.; Boudreaux, D. S.; Chance, R. R. Chain-Length Dependence of Electronic and Electrochemical Properties of Conjugated Systems: Polyacetylene, Polyphenylene, Polythiophene, and Polypyrrole. *J. Am. Chem. Soc.* **1983**, *105*, 6555–6559.
(6) Miyamoto, E.; Yamaguchi, Y.; Yokoyama, M. Ionization Potential of Organic Pigment Film by Atmospheric Photoelectron Emission Analysis. *Electrophotography* **1989**, *28*, 364–370.
(7) Kukhta, N. A.; Volyniuk, D.; Peciulyte, L.; Ostrauskaite, J.; Juska, G.; Grazulevicius, J. V. Structure–property Relationships of Star-Shaped Blue-Emitting Charge-Transporting 1,3,5-Triphenylbenzene Derivatives. *Dyes Pigm.* **2015**, *117*, 122–132.
(8) Mimaite, V.; Grazulevicius, J. V.; Laurinaviciute, R.; Volyniuk, D.; Jankauskas, V.; Sini, G. Can Hydrogen Bonds Improve the Hole-Mobility in Amorphous Organic Semiconductors? Experimental and Theoretical Insights. *J. Mater. Chem. C* **2015**, *3*, 11660–11674.
(9) Forrest, S. R.; Bradley, D. D. C.; Thompson, M. E. Measuring the Efficiency of Organic Light-Emitting Devices. *Adv. Mater.* **2003**, *15*, 1043–1048.
(10) Baldo, M.; Forrest, S.; Thompson, M. Organic Electrophosphorescence. In *Organic Electroluminescence*; Kafafi, Z., Ed.; CRC Press, **2005**; 267–305.